Kinetics of ultrashort relativistic electron pulses emitted from solid targets

Ernst E. Fill
Max-Planck-Institut für Quantenoptik, D-85748 Garching, Germany
(Received 31 March 2004; revised manuscript received 18 June 2004; published 28 September 2004)

Interaction of ultrashort high-intensity laser pulses with solid targets generates relativistic electrons which escape from the target. The kinetics of these ultrashort electron pulses is governed by self-fields generated by the charge of the electron cloud. In this paper an analytical theory is developed which allows calculation of electron trajectories, electron fluxes, and electron spectra at any distance from the target. The theory is exact for two limiting cases: (a) a monoenergetic electron pulse with an arbitrary temporal shape; (b) an infinitely short electron pulse with an arbitrary energy spectrum. These results have applications in high-intensity irradiation experiments, e.g., in experiments irradiating samples with ultrashort electron or x-ray pulses, in developing optics for fourth-generation light sources, and in work relating to x-ray lasers.

DOI: 10.1103/PhysRevE.70.036409 PACS number(s): 52.20.Dq, 52.27.Ny, 52.38.Kd

I. INTRODUCTION

It is well known that interaction of a high-intensity laser pulse with a solid target generates intense electron pulses [1–5]. These electrons are seen to escape from the front side of the material as well as to propagate into the material. Highly collimated beams with a velocity close to light velocity have been reported [6,7]. Experimental and theoretical features of propagation of laser-generated electron beams through solids and dense plasmas are reasonably well understood [8–11]. However, our understanding of the transition of high-current electron beams from the conductor into a vacuum is much less complete. Straightforward application of the Poisson equation predicts that large electrostatic fields are generated, slowing down the electrons or entirely preventing their propagation. Thus, the farther away from the target a sample to be irradiated is positioned, the fewer electrons are expected to hit the sample and the more the effect of the x rays dominates. Quantitative knowledge of the number of electrons and their energy distribution is essential for separating the effects of the x rays from those of the electrons. This is crucial for utilizing laser-generated intense x rays for irradiating samples, e.g., in developing optics for fourth-generation light sources and pumping x-ray lasers [4,5,12].

Typically, in such experiments the radiation source should be approached as closely as possible in order to obtain a high radiation dose. Experiments with source-sample distances of $50-100$ μm are state of the art [4,13] but smaller distances are desirable. If the gap between source and sample is smaller than the source diameter, the geometry is planar and the x-ray dose becomes independent of the distance. However, as will be shown in this paper, the electron dose is strongly dependent on the gap width.

In previous work, analytical theories were developed for the case of a monoenergetic electron beam which is constant in time [14] or rises with a power law [15]. Furthermore, the case of an infinitely short electron pulse with a flat distribution of energies [16] and with an energy spectrum [17] was developed.

In this paper the theory of Ref. [17] is further developed and two limiting cases—monoenergetic electrons with an *arbitrary temporal shape* and instantaneously released electrons with an *arbitrary energy spectrum*—are treated in a unified way. The results are then used to calculate important features, such as the fraction of electrons propagating beyond a certain distance from the target, and electron spectra at a distance from the target. The theory is based on solving the Poisson equation and the equation of motion of the electrons simultaneously, using a Lagrangian coordinate for the electrons.

Applicability of the theory is limited to the region in which the Lagrangian description is viable. It should be kept in mind that electrons reflected close to the target surface form a "virtual cathode" for which the electron flow is no longer laminar and for which the Lagrangian coordinate breaks down. Nevertheless, it will turn out that the region where the theory is applicable covers the greater part of the spatiotemporal domain.

II. MONOENERGETIC ELECTRON BEAM WITH ARBITRARY TEMPORAL SHAPE

Consider a planar one-dimensional electron beam with an areal density N_a entering a vacuum from a conducting solid. The electron flux as a function of time is given by $\eta_b(t)$ and is related to the areal density of the electrons by

$$N_a = \int_0^\infty \eta_b dt. \tag{1}$$

A Lagrangian coordinate ξ for the electrons is defined by

$$\xi(t) = \frac{1}{N_a}\int_0^t \eta_b dt', \tag{2}$$

which ranges between 0 and 1 and denotes the fraction of electrons emitted up to a time t. Closed form solutions are anticipated if $\eta_b(t)$ can be integrated and the integral function can be inverted. This is the case for many practical functions, such as exponential decay and the Lorentzian and so-called Rayleigh functions to be discussed later.

The system considered is globally charge neutral: A positive surface charge on the boundary of the conductor equal to

the charge of the electron cloud provides global charge neutrality and makes the field zero in the conductor. Thus, the field is zero in the conductor, sharply rises close to the boundary, has a maximum at the boundary itself, and then slowly decays along the electron cloud to become zero again at the outermost particle. It then stays zero up to infinity.

For an electron population with Lagrangian coordinate ξ the areal density of electrons further out from the target is given by ξN_a. The Poisson equation then yields for the electric field in the vacuum region

$$E = 4\pi e \xi N_a, \tag{3}$$

where e is the elementary electric charge (see the Appendix for a rigorous derivation). The equation of motion becomes

$$\frac{\partial \beta}{\partial t} = -4\pi e^2 \xi N_a/(mc\gamma^3). \tag{4}$$

In this equation β is the particle velocity divided by c, c is the light velocity, m is the electron rest mass, and $\gamma=(1-\beta^2)^{-1/2}$ is the relativistic mass factor.

It is advantageous to go over to dimensionless variables by introducing the definitions

$$\tau = t/t_n, \quad X = x/x_n \tag{5}$$

with the normalization parameters $t_n=(4\pi c r_e N_a)^{-1}$ and $x_n=(4\pi r_e N_a)^{-1}$. Here $r_e=e^2/mc^2=2.82\times10^{-13}$ cm is the classical electron radius. As an example, at a typical experimental areal density of $N_a=10^{15}$ cm^{-2} one has $x_n=2.8$ μm and $t_n=9.3$ fs. With these definitions Eq. (4) transforms to

$$\frac{\partial \beta}{\partial \tau} = -\xi(1-\beta^2)^{3/2}. \tag{6}$$

Integration of Eq. (6) yields

$$\frac{\beta}{(1-\beta^2)^{1/2}} = -\xi\tau + C_1. \tag{7}$$

Using the initial condition that $\beta=\beta_0$ for $\tau=\tau_0(\xi)$, where $\tau_0(\xi)=t_0(\xi)/t_n$ and $t_0(\xi)$ is the inverse of $\xi(t)$ defined in Eq. (2), one obtains for the integration constant $C_1=\beta_0\gamma_0+\xi\tau_0(\xi)$. This yields the final solution for β:

$$\beta(\xi,\tau) = \frac{\beta_0\gamma_0 + \xi\tau_0(\xi) - \xi\tau}{\{[\beta_0\gamma_0 + \xi\tau_0(\xi) - \xi\tau]^2 + 1\}^{1/2}}. \tag{8}$$

Further integration over τ using the boundary condition that $X=0$ for $\tau=\tau_0(\xi)$ results in the solution for X:

$$X(\xi,\tau) = \frac{1}{\xi}\{\gamma_0 - [(\beta_0\gamma_0 + \xi\tau_0(\xi) - \xi\tau)^2 + 1]^{1/2}\}. \tag{9}$$

To illustrate the significance of Eq. (9), Fig. 1 shows particle trajectories for the example of a Rayleigh pulse, given in normalized form by

$$\eta_b(\tau) = \tau/\tau_{\max}^2 \exp(-\tau^2/2\tau_{\max}^2). \tag{10}$$

This pulse has a maximum at $\tau_{\max}$ with a pulse half-width given by $1.6\tau_{\max}$. Inserting Eq. (10) in Eq. (1), it is easily realized that for this function the expression for $\tau_0(\xi)$ [to be inserted in Eqs. (8) and (9)] becomes $\tau_0(\xi)=\tau_{\max}[-2\ln(1-\xi)]^{1/2}$. Figure 1 shows space-time trajectories for the particular case of $\mathcal{E}_{el}=500$ keV, $\tau_{\max}=2$, and values of $\xi=0.001$, 0.1, 0.3, …up to 0.9. The pulse is also drawn in the figure. The electrons released at later times (with ξ increasing) exhibit shorter and shorter orbits due to the rising self-fields. The breakdown of the Lagrangian coordinate is seen to occur at $\xi=0.8$, for which value two curves cross each other. In the greater part of the spatiotemporal domain, however, the Lagrangian coordinate is sound and the theory is applicable.

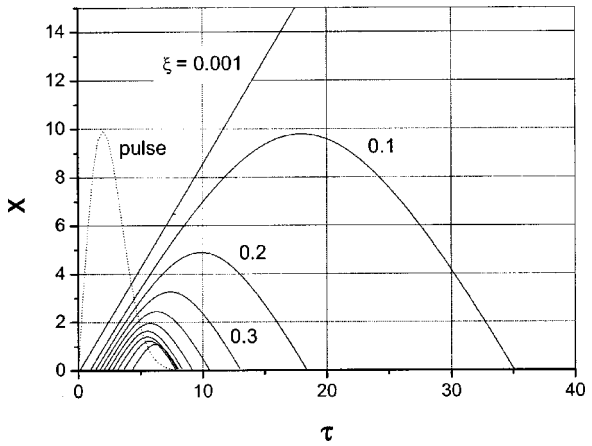

FIG. 1. Electron trajectories for a monoenergetic "Rayleigh" pulse for $\tau_{\max}=2$ (drawn dotted) with the Lagrangian coordinate ξ as a parameter. The initial electron energy is 500 keV. The space and time coordinates are dimensionless. Curves are drawn for $\xi=0.001$, 0.1, 0.2,… up to 0.9. The curve with $\xi=0.8$ is seen to cross the curve with $\xi=0.9$, indicating breakdown of the Lagrangian coordinate description.

III. INSTANTANEOUSLY RELEASED ELECTRONS WITH ARBITRARY ENERGY DISTRIBUTION

This second limiting case can be treated in close analogy to the first one. Again, a Lagrangian coordinate for the electrons is used, with the new definition

$$\xi(U) = \int_U^\infty f(U')dU'. \tag{11}$$

Here U is the energy of the electrons and $f(U)dU$ is their normalized energy distribution. From its definition $\xi(U)$ ranges from 0 to 1 and gives the fraction of the electrons with an energy greater than U. Note the difference in the limits of the integral with respect to Eq. (1); this choice of limits is advantageous to render the formalism as similar as possible to that in the previous section.

To make the situation more general it is assumed that the electrons first propagate uninhibited through a foil of thickness d. (For electrons that emerge from the front side of a target one may take $d=0$.) If the electrons start instantaneously, particles cannot overtake each other. Thus, at a distance x from the solid, the Lagrangian coordinate ξ denotes the fraction of the electrons that has propagated beyond that

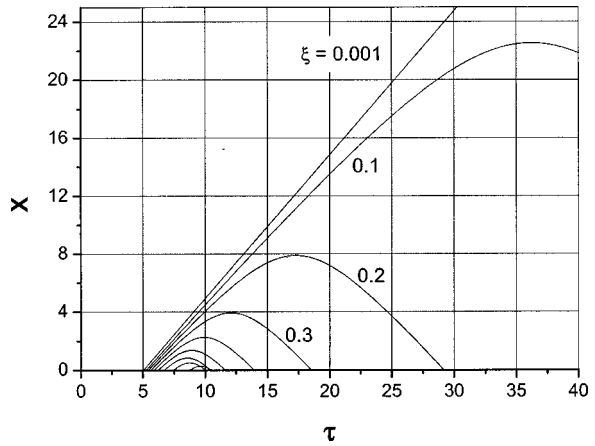

FIG. 2. Electron trajectories for an infinitely short electron pulse with an exponential energy distribution. The space and time coordinates are dimensionless. Electron temperature $kT_e=500$ keV. The electrons are released at the rear of a foil with a normalized thickness $D=5$. Curves are drawn for $\xi=0.001$, 0.1, 0.2,… up to 0.8. The curve with $\xi=0.7$ is seen to cross the curve with $\xi=0.8$, indicating breakdown of the Lagrangian coordinate description.

distance. Similarly to the previous section, integration of the Poisson equation (see the Appendix) yields the field at position x as given by $E(x)=4\pi e\xi N_a$, and electrons with Lagrangian coordinate ξ experience a decelerating force given by $-4\pi e^2\xi N_a$. With the same normalization as previously the equation of motion is again given by Eq. (6), integration of which leads to Eq. (7). However, now the boundary condition is different and the integration constant C_1 is derived from the condition that the particles have a velocity β_0 at a time $t=d/\beta_0 c$, i.e., at $\tau=D/\beta_0$, where $D=d/x_n$ is the dimensionless foil thickness. With this boundary condition, solving for β one obtains

$$\beta(\xi,\tau)=\frac{\gamma_0\beta_0+\xi D/\beta_0-\xi\tau}{[(\gamma_0\beta_0+\xi D/\beta_0-\xi\tau)^2+1]^{1/2}}. \tag{12}$$

Further integrating, using the boundary condition $X=0$ at $\tau=D/\beta_0$, yields the trajectory

$$X(\xi,\tau)=\frac{1}{\xi}\{\gamma_0-[(\gamma_0\beta_0+\xi D/\beta_0-\xi\tau)^2+1]^{1/2}\}. \tag{13}$$

The similarity of Eqs. (12) and (13) to Eqs. (8) and (9) for the monoenergetic case is obvious. However, in Eqs. (12) and (13) β_0 and γ_0 are functions of ξ in a way depending on the electron energy distribution. The significance of Eq. (13) is illustrated in Fig. 2, which displays orbits with increasing ξ for the particular case of an exponential energy distribution. A temperature $kT_e=500$ keV is chosen and the dimensionless foil thickness $D=5$. The finite foil thickness results in the starting points of the orbits being displaced by the time taken by the different electron populations to traverse the foil. The first orbit, with $\xi=0.001$, starts at $\tau=5$, which is just the normalized time an electron with $\beta=1$ needs to traverse the foil. Again, for $\xi>0.7$, in a small region near the target the description with a Lagrangian coordinate breaks down. In the greater part of the spatiotemporal domain, however, the Lagrangian description is justified.

IV. APPLICATIONS

A. Fraction of electrons beyond a certain distance from the target

An important application of the above theory is calculation of the fraction of electrons that propagate beyond a certain distance from the target. This is achieved by realizing that the maximum distance of the electrons with Lagrangian coordinate ξ is determined by the condition $\beta=0$. The fraction of electrons to be found beyond that distance is thus given by $\xi(\beta=0)$. Applying this condition to Eqs. (7) and (12) and inserting into Eqs. (8) and (13), respectively, one obtains the equation

$$X_{\max}(\xi)=(\gamma_0-1)/\xi, \tag{14}$$

and thus the fraction of electrons propagating beyond X is given by

$$\xi=(\gamma_0-1)/X. \tag{15}$$

It should be noted that in the case of a monoenergetic electron beam, Eq. (15) is a simple algebraic equation, whereas for a beam with an electron energy distribution γ_0 depends on ξ, and therefore the equation in general becomes transcendental. For example, an exponential electron energy distribution yields $U=-kT_e\ln\xi$ for the kinetic energy and thus

$$\gamma_0=1-\frac{kT_e}{mc^2}\ln\xi. \tag{16}$$

Therefore Eq. (15) becomes

$$\xi=-\frac{kT_e}{mc^2}\frac{\ln\xi}{X}. \tag{17}$$

In Fig. 3 the results of Eqs. (15) and (17), viz., the fractions of electrons bridging a vacuum gap behind the target, are plotted for $kT_e=200$, 500, and 1000 keV (exponential energy distribution) and for $\mathcal{E}_{el}=200$, 500, and 1000 keV (monoenergetic beam). To make the results better applicable to a real situation an areal density of $N_a=10^{15}$ cm^{-2} is chosen and the distance scale is in micrometers.

B. Electron energy spectrum at a distance from the target

The introduction of a Lagrangian coordinate allows calculation of the energy spectrum of the electrons at any distance from the target: Electrons with Lagrangian coordinate ξ lose a kinetic energy $\Delta U=4\pi e^2 x\xi N_a$ after they have propagated a distance x away from the target. In normalized quantities, the energy loss is given by $\Delta U=mc^2X\xi$ and thus the remaining energy of these electrons is given by

$$U=U_0-mc^2X\xi. \tag{18}$$

Differentiating with respect to ξ one obtains

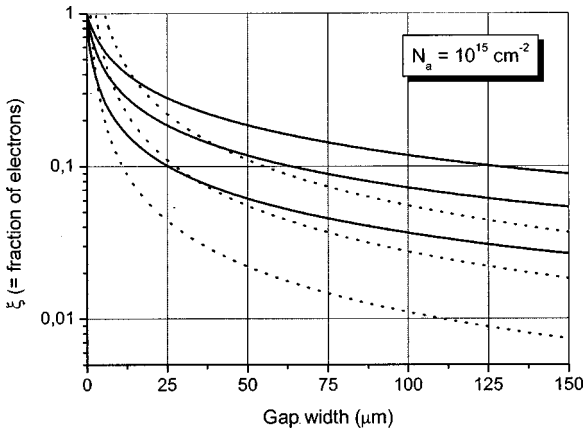

FIG. 3. Fraction of electrons crossing a gap. The curves are drawn for real coordinates and an areal electron density of 10^{15} cm^{-2}. Dotted curves are for monoenergetic electrons with electron energies of 200, 500, and 1000 keV (from bottom). These curves are seen to originate at a small distance from the target, a consequence of the breakdown of the Lagrangian coordinate description. Solid curves are for exponential electron energy distributions with kT_e=200, 500, and 1000 keV (from bottom).

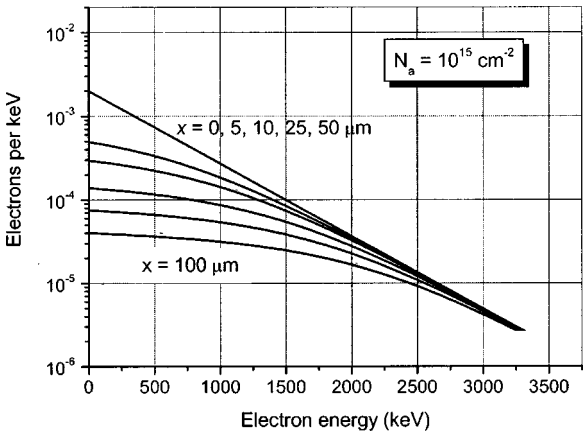

FIG. 4. Electron spectra at various distances from the target. The curves are drawn for real coordinates and an areal electron density of 10^{15} cm^{-2}. The input spectrum (at x=0) is exponential with a temperature of 500 keV. Further spectra are shown (from top) at distances x=5, 10, 25, 50, and 100 μm from the target.

$$\frac{\partial U}{\partial \xi} = \frac{\partial U_0}{\partial \xi} - mc^2 X. \tag{19}$$

From Eq. (11) the fraction of electrons in any energy interval dU is given by $-(\partial\xi/\partial U)dU$ and thus the energy spectrum of the electrons is obtained by varying ξ from 0 to 1 and plotting $-\partial\xi/\partial U = -1/(\partial U/\partial\xi)$ from Eq. (19) vs U.

For an exponential energy distribution the expressions (18) and (19) become quite simple, yielding

$$U = -kT_e \ln \xi - mc^2 \xi X \tag{20}$$

and

$$-\frac{\partial U}{\partial \xi} = kT_e/\xi + mc^2 X. \tag{21}$$

In Fig. 4 electron spectra at different distances from the target are displayed. Again, to make the figure more applicable to a real experiment, the areal density of the electrons is specified at 10^{15} cm^{-2} and real distances (in micrometers) rather than normalized ones are plotted. One can see how the original spectrum (at x=0) is altered upon increasing the distance from the target. Note that the electron distribution is normalized to the distribution at x=0, and thus at a distance from the target the number of electrons is reduced.

V. CONCLUSIONS AND LIMITATIONS OF APPLICABILITY

The above theory shows that the description of electrons by means of a Lagrangian coordinate allows analytical calculation of electron kinetics subject to self-generated fields. Electron trajectories, electron transmissions, and spectra can easily be determined. Experimental conditions for which the theory is applicable include electrons emerging from the front side of an irradiated target and electrons emerging into a vacuum after propagating through a metallic foil.

Application of the theory to conditions encountered in experiments reveals that the fraction of electrons crossing a narrow gap very much depends on the electron temperature. A typical experimental areal electron density is $N_a = 10^{15}$ cm^{-2}. Inspection of Fig. 3 shows that, under this condition and for an initially exponential distribution with kT_e =200 keV, only 10% of the electrons reach a distance of 25 μm from the target surface. However, for kT_e=500 keV that fraction is twice as large, and for 1 MeV it is about tripled.

The spectra derived from the theory show that the high-energy tail of the electron energy distribution is much less reduced than the low-energy part. With $N_a = 10^{15}$ cm^{-2} again being used, an initially exponential spectrum with kT_e =500 keV is significantly deprived of low-energy electrons (see Fig. 4). At a distance of 25 μm the number of electrons below 100 keV is down by a factor of about 10, whereas the number of 1 MeV electrons is reduced by a factor of less than 3. The high-energy tail above 3 MeV is almost unaffected even at a distance of 100 μm from the target.

A relatively simple analytical theory such as this one is subject to a number of limitations. It should be kept in mind that the theory breaks down in a region where the Lagrangian formalism is no longer applicable. This occurs at the time when electrons begin to be reflected close to the target surface. As a consequence, electron trajectories cross each other and a "virtual cathode" is formed. Fortunately, as inspection of Figs. 1 and 2 reveals, this happens only in a very limited spatiotemporal domain, and thus the theory is valid in the greater part of space and time.

A further limitation of applicability arises due to the planar geometry. It limits the distance from the target at which the theory is applicable to about the diameter of the beam. At larger diameters expansion of the beam in the radial direction will decrease the electric field and permit more electrons to escape from the target. In addition, magnetic field effects will gain in importance in relation to the purely electrostatic effects considered here.

Another point of concern is the plasma formed at the target. Plasmas are generated on the front and rear sides of targets (see, for example, [2]). Formation of a plasma rules out applicability of the theory in this region. Fortunately, the expansion velocity of a plasma is of the order of the ion acoustic velocity, and therefore the disturbed range is quite small for the time scales considered in this paper. However, for longer time scales plasma expansion and the appearance of accelerated ions will alter the space charge distribution at increasing distances from the target. Further analysis would be necessary to take the effects of plasma formation fully into account.

Obviously, the condition of instantaneous release of the electrons required for the case of the electron energy distribution treated in Sec. III is better satisfied for shorter pulse duration. The theory is still approximately applicable at a distance x from the target if the pulse duration satisfies $\tau_p \ll x/c$. It is easily appreciated that this is a precondition for a Lagrangian coordinate treatment to apply.

ACKNOWLEDGMENT

This work was supported in part by the European Communities in the framework of the Euratom-IPP Association.

APPENDIX

To prove that the electric field at a Lagrangian coordinate ξ is given by Eq. (3) the integral of Eq. (2) is transformed into an integral over the spatial coordinate x. Using $dt = -dx/u$, where u is the velocity of the particles, one obtains

$$\xi = \frac{1}{N_a}\int_0^t \eta_b dt' = -\frac{1}{N_a}\int_{x_{\max}}^{x(\xi)} \frac{\eta_b}{u} dx', \tag{A1}$$

where $x_{\max} = x(\xi = 0)$. Realizing that the beam electron density n_b is given by η_b/u, Eq. (A1) is written as

$$\xi = \frac{1}{N_a}\int_{x(\xi)}^{x_{\max}} n_b dx', \tag{A2}$$

and integration of the Poisson equation leads directly to Eq. (3) for the field,

$$E = 4\pi e \xi N_a. \tag{A3}$$

The negative charge of the electrons results in the positive sign in Eq. (A3).

Similarly, the integral of Eq. (11) can be transformed into an integral over space by the substitution $f(U)dU = dN_a/N_a = n_b d_x/N_a$. Equation (11) then becomes

$$\xi = \int_U^\infty f(U')dU' = \frac{1}{N_a}\int_{x(\xi)}^{x_{\max}} n_b dx' \tag{A4}$$

from which again Eq. (A3) follows. In Eqs. (A2) and (A4) use has been made of the fact that the number of particles between two Lagrangian coordinates is constant, and thus for fixed ξ_1 and ξ_2 the integral $\int_{x(\xi_1)}^{x(\xi_2)} n_b dx'$ is independent of time and space.

[1] F. N. Beg, A. R. Bell, A. E. Dangor, C. N. Danson, A. P. Fews, M. E. Glinsky, M. E. Hammel, P. Lee, P. A. Norreys, and M. Tatarakis, Phys. Plasmas **4**, 447 (1997).

[2] M. Tatarakis, J. R. Davies, P. Lee, P. A. Norreys, N. G. Kassapakis, F. N. Beg, A. R. Bell, M. G. Haines, and A. E. Dangor, Phys. Rev. Lett. **81**, 999 (1998).

[3] K. B. Wharton, S. P. Hatchett, S. C. Wilks, M. H. Key, J. D. Moody, V. Yanovsky, A. A. Offenberger, B. A. Hammel, M. D. Perry, and C. Joshi, Phys. Rev. Lett. **81**, 822 (1998).

[4] G. Pretzler, T. Schlegel, and E. Fill, Laser Part. Beams **19**, 91 (2001).

[5] G. Pretzler, T. Schlegel, E. Fill, and D. C. Eder, Phys. Rev. E **62**, 5618 (2000).

[6] M. Borghesi, A. J. Mackinnon, A. R. Bell, G. Malka, C. Vickers, O. Willi, J. R. Davies, A. Pukhov, and J. Meyer-ter-Vehn, Phys. Rev. Lett. **83**, 4309 (1999).

[7] L. Gremillet, F. Amiranoff, S. D. Baton, J.-C. Gauthier, M. Koenig, E. Martinolli, F. Pisani, G. Bonnaud, C. Lebourg, C. Rousseaux, C. Toupin, A. Antonicci, D. Batani, A. Bernardinello, T. Hall, D. Scott, P. Norreys, H. Bandulet, and H. Pepin, Phys. Rev. Lett. **83**, 5015 (1999).

[8] J. R. Davies, A. R. Bell, and M. Tatarakis, Phys. Rev. E **59**, 6032 (1999).

[9] H. Ruhl, Y. Sentoku, K. Mima, K. A. Tanaka, and R. Kodama, Phys. Rev. Lett. **82**, 743 (1999).

[10] E. Fill, Phys. Plasmas **8**, 1441 (2001).

[11] J. J. Santos, F. Amiranoff, S. D. Baton, L. Gremillet, M. Koenig, E. Martinolli, M. Rabec Le Gloahec, C. Rousseaux, D. Batani, A. Bernardinello, G. Greison, and T. Hall, Phys. Rev. Lett. **89**, 025001 (2002).

[12] D. C. Eder, G. Pretzler, E. Fill, K. Eidmann, and A. Saemann, Appl. Phys. B: Lasers Opt. **70**, 211 (2000).

[13] J. Stein, E. Fill, D. Habs, G. Pretzler, and K. Witte, Laser Part. Beams (to be published).

[14] J. W. Poukey and N. Rostoker, Plasma Phys. **13**, 897 (1971).

[15] J. W. Hantzsche, Beitr. Plasmaphys. **15**, 157 (1975).

[16] A. E. Dubinov, Plasma Phys. Rep. **26**, 409 (2000).

[17] E. Fill, Phys. Plasmas **8**, 4613 (2001).